Carbon Nano-Octopi: Growth and Characterisation

Monica S. Saavedra

Submitted in partial fulfilment of the requirements for the degree of Engineering Doctorate in Micro- and Nano-Materials and Technologies (EngD)

April 2014

Faculty of Engineering & Physical Sciences
Division of Mechanical, Medical and Aerospace Engineering
Guildford, Surrey GU2 7XH, UK

Abstract

This work focuses on the conditions under which multiple carbon nano-fibres (CNFs) can be grown radially on a single metal catalyst, known as carbon nano-octopi (CNO) structures, and expands on the evaluation for this type of growth in order to produce large surface areas at the low temperatures that are compatible with large area electronic processing. It was found that the CNF growth was promoted by the use of an adhesive tape initially utilised to fasten a carbon cloth coated with a nickel catalyst onto a silicon support. Compositional characterisation of the catalyst using electron energy loss spectroscopy (EELS), revealed copper in the bulk of the nickel catalyst and in some surface locations near the catalyst edges. An investigation of the growth mechanism was necessary to increase the CNO yield and produce homogeneous large-area growth, and was facilitated by the control and reduction of the number of experimental parameters in the growth runs. It was observed that CNO growth can occur under a range of temperatures and copper to nickel ratios, however, the growth resulted in a single CNF per catalyst in the absence of the polymer, the copper metal and/or in the case of a large copper to nickel ratio on the catalyst surface. Growth would not occur at all in the absence of acetylene. It was concluded that both the copper and the polymer of the adhesive played a role in the growth mechanism of the CNOs: the polymer enabled catalyst faceting, allowing for multiple carbon leg formation, and the active nickel regions on the surface of the cupro-nickel catalyst served to separate the growing carbon legs.

Maximising the specific yield and surface area of carbon nanostructures can help to improve the efficiency of a range of devices. CNO forests with higher yields and higher specific surface areas were achieved by optimising growth parameters such as temperature, catalyst annealing time and catalyst thickness. It was found that the radial growth of thinner, longer, more numerous legged CNOs is promoted by the choice of the size of the catalysts on which they are grown. It was also found that the diameter and length of the nanofibres depend on the catalyst diameter which can be tuned by controlling the annealing time of the catalyst. The surface area that can be obtained from the octopus geometry was optimised at a critical catalyst size of 125 nm through growth of a large number of octopus legs. Carbon films consisting of CNOs resulted in relatively low electrical resistivity, highlighting the possibility of their use as high surface area electrical contacts.

Acknowledgments

The work was carried out as part of an Engineering Doctorate Programme in Micro- and NanoMaterials and Technologies, financially supported by the EPSRC, the University of Surrey and the National Physical Laboratory (NPL). The author would like to thank Dr Vladimir Stolojan and Dr Robert Boyd for carrying out electron energy loss spectroscopy (EELS) studies, Dr Jose Anguita for the some of the growth and training given on the thermal and photo-thermal chemical vapour deposition (PTCVD) systems, Dr Felicia Green for material studies on the time of flight secondary ion mass spectrometer (ToF SIMS), Sam Gnaniah for the training given on the Thermogravimetric analyser (TGA), Steve Spencer for access to and training on the ellipsometer and Hugh Davies for access and consultation on the MTDATA database system. Many more scientists are to be acknowledged and thanked for their contributions, however, I would exhaust a page or two in doing so.

This thesis would not have been possible without the help and support of the supervisory team from the NPL, Prof. Graham Sims and Prof. Neil McCartney and the supervisory team from the University of Surrey, Prof. Ravi Silva (Advanced Technology Institute), Prof. Steve Ogin and Prof. Paul Smith (Division of Mechanical, Medical and Aerospace Engineering), who were always there to offer their comparatively infinite knowledge and help manage my 'student-like' daily routines.

The encouragement, enthusiasm and expectations of my family helped me to see this work through to the end, and the momentum needed to persevere was possible only thanks to the many cups of tea and words of wisdom from my partner Steven King.

Table of Contents

Glossary

AC	Activated carbon
ACF	Activated carbon fabric
ATI	Advanced Technology Institute
BE	Backscattered electron
C	Carbon
CB	Carbon black
CC	Carbon cloth
CF	Carbon fibre
CNS	Carbon nanostructure
CNF	Carbon nanofibre
CNT	Carbon nanotube
CNO	Carbon nano-octopus
CO_x	Carbon oxides, where x = 1, 2, 3 (the latter is less common)
C_2H_2	Acetylene
C_2H_4	Ethylene
Cu	Copper
Cu_xC_y	Copper carbide
Cu_2C_2	Copper acetylide
CuNi	Cupronickel or copper-nickel
Cu:Ni	Copper on nickel bi-layer structure
CVD	Chemical vapour deposition
DFT	Density-functional theory
EELS	Electron energy loss spectroscopy
EDX	Energy dispersive X-rays
ETEM	Environmental transmission electron microscope

FCC	Face centred cubic
FE	Field emission
FFT	Fast Fourier transform
H_2	Molecular hydrogen
HR-TEM	High-resolution transmission electron microscopy
ICSD	Inorganic crystal structure database
IR	Infrared
MD	Molecular dynamics
MFC	Mass flow controller
MSDS	Material safety datasheet
Ni	Nickel
Ni:Cu	Nickel on copper bi-layer structure
NiO	Nickel oxide
NIST	National institute for science and technology
NO_x	Nitrogen oxides, where x = 1, 2
NPL	National Physical Laboratory
O	Oxygen
OPV	Organic photovoltaic
PAN	Polyacrylonitrile
PTCVD	Photo-thermal chemical vapour deposition
RGB	Red, green and blue
SC	Supercapacitor
sccm	Standard cubic centimetre per minute
SE	Secondary electrons
SEM	Scanning electron microscope
Si	Silicon
SiO_2	Silicon dioxide

SWNT	Single walled nanotube
TEM	Transmission electron microscopy
TGA	Thermogravimetric analyser
ToF SIMS	Time of flight secondary ion mass spectroscopy
V-L-S	Vapour-liquid-solid (gaseous feedstock, liquid catalyst, solid carbon structure)
V-S-S	Vapour-solid-solid (gaseous feedstock, solid catalyst, solid carbon structure)
XPS	X-ray photoelectron spectroscopy

Symbols

Å	Angstrom (1×10^{-10} m)
ε	Activation energy of diffusion (eV)
ρ_o	Density of octopi (number of octopi per unit meter)
λ	Diffusion length (cm)
at%	Atomic percent (%)
D	Temperature dependent diffusion (cm^2s^{-1})
D_0	Diffusion coefficient (cm^2s^{-1})
d_L	Carbon nano-octopus leg diameter (nm)
H_f	Enthalpy of formation
k_B	Boltzmann's constant ($1.3806488 \times 10^{-23}$ JK^{-1})
M	Mole
M_w	Molecular weight (dimensionless)
N_A	Avogadro's number (6.023×10^{23})
r	Filament growth rate (ms^{-1})
r_0	Filament growth rate prefactor (ms^{-1})
T_m	Melting temperature (°C)
wt %	Weight percentage (%)
Z	Atomic number (number of protons) of a chemical element

1 Introduction

1.1 Background

The development of new technological devices continuously brings improvements to personal devices like telephones and computers, which have evolved to portable devices, such as mobile phones and tablets, over the course of little more than a century. Rapid miniaturisation for enhanced device mobility has approximately halved the size of parts while doubling the overall device performance each year (Moore's law [1]), leading to fabrication methods with nano-scale accuracy.

Some of the smallest functional components in portable devices are nanomaterials, consisting of zero dimensions (e.g. quantum dots) with a width, height and length between 1 nm and 100 nm in size; or two dimensions (i.e. nanofibres), with a diameter between 1 nm and 100 nm and a length between a few hundreds of nanometres and a few centimetres [2]. Nanomaterials have been used in a variety of applications, from nanocomposites for armour reinforcement to as-grown electrodes for flexible solar cells. The properties of nanoscale materials can differ vastly from that of their macroscopic counterparts, often as a consequence of enhanced surface interactions or quantum confinement. Chemical, electrical, thermal and mechanical properties can all be modified as a consequence of a larger number of surface atoms to bulk atoms and nearly perfect, well-defined atomic structures. The large number of surface atoms to bulk atoms ratio gives rise to properties such as higher surface areas, higher chemical activity and lower melting temperatures; the near structural perfection and nano-size gives rise to ballistic (scatter-free) electric and thermal conductivity, quantised conductance [3], negative resistance, transparency and/or colour change via surface plasmon resonance [4,5].

An important category of nanomaterials are carbon nanostructures, allotropes of carbon which consist of single or multiple graphene layers. Graphene itself is a planar allotrope of carbon, having carbon atoms arranged in repeated hexagonal ring patterns, as shown in Figure 1.1.

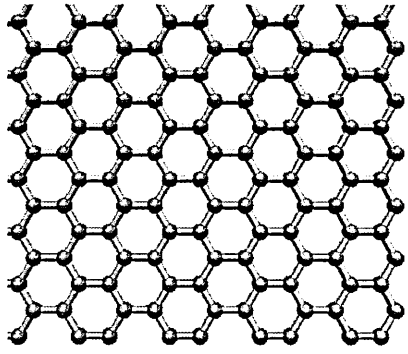

Figure 1.1 *Graphene, the planar allotrope of carbon.*

The history of carbon nanostructures begins in 1985, when the Buckminsterfullerene C_{60} was discovered by Kroto *et al.* [6]. Since then, the number of discovered structures increased rapidly. Some examples of nanostructures include carbon nanotubes, discovered by Ijima [7], the family of fullerenes C_{70}, C_{76} [8], C_{84} [9], carbon nanocones [10], carbon nanohorns [7], nanoscale carbon toroidal structures [11] and helicoidal tubes [8,12], amongst others. These carbon structures could be single-walled or multi-walled. A well-known carbon nanostructure that satisfies most of the aforementioned desirable properties and vast range of applications, is the carbon nanotube (CNT). This is a tube comprising a single or multiple concentric graphene sheets. Carbon nanotubes consisting of a single tube of graphene are known as single walled carbon nanotubes, or SWNT (see Figure 1.2d), with diameters ranging between 0.3 nm [13] and 10 nm [14]. Carbon nanotubes comprising multiple concentric graphene tubes are known as multi walled carbon nanotubes, or MWNT (see Figure 1.2e), with diameters ranging between 0.7 nm [15] to 200 nm [16]. In MWNTs the diameter is largely dependent on the number of graphene walls. CNT lengths range between a few nanometres and several centimetres [17], but are typically grown to a few to several microns. The excellent electrical, thermal and mechanical properties as well as the light-weight and flexible nature of CNTs are derived from their atomic structure and nano-size.

Since the first accurate account of the CNT structure in 1991 [7], research efforts returned to carbon nanostructures such as carbon nanofibres (CNFs), originally manufactured in, perhaps, 1889 by T. V. Hughes and C. R. Chambers [18] and their structure characterised by T. Koyama and M. Endo in 1973 [19]. Nanofibres can be used for applications similar to those achievable by CNTs. CNFs are often several times larger in diameter compared to CNTs and consist of multiple stacked graphene layers. The stacking of graphene layers can offer advantages such as high surface areas as well as disadvantages such as non-ballistic conduction. CNFs can be used in applications such as supercapacitors and hydrogen storage, where the morphological and physicochemical properties of CNFs can be tailored further to optimise device performance.

Porous carbon nanostructures (CNSs) are gaining attention due to their large surface areas that allow for potential applications such as complex architectures on electrodes for chemical and gas sensing, energy storage and conversion devices, gas separation, hydrogen storage and water purification [20,21]. Like CNTs, porous nanostructures can be grown adjacent to each other and perpendicular to a substrate to form a forest-like geometry, allowing for nano-patterned electrodes with large surface areas capable of adsorbing 68 wt.% hydrogen [22]. The high surface areas of the nanostructured surfaces can increase the functionality and efficiency of a device. In the case of supercapacitors, organic solar cells and gas sensors, a higher surface area translates to higher capacitance, higher charge collection efficiency and larger hydrogen storage, respectively. Carbon nanostructures can help reduce the cost of devices such as hydrogen storage and supercapacitors (SCs) by substituting costly metals with carbon, of which nanostructures are grown with well-established and low-cost manufacturing methods. Additionally carbon nanostructures have physical advantages over metals owing to the weak van der Waals forces present between the adsorbed atoms or molecules, enabling more efficient desorption when required [23].

1.2 Carbon Structures

Since the first carbon filament growth observations, made over 120 years ago (Schutzenberger, 1890), several types of CNSs have been achieved, including graphene nano-ribbons [24], single-walled CNTs [7], buckminsterfullerenes and carbon nano-scrolls [25], all consisting of a single graphene layer arranged in different geometries such as a rectangular shape, rolled-up into a tube, a sphere or a scroll. These CNSs are defined as nano-sized owing to their nano-sized widths, often between 1 nm and 100 nm [2]. CNFs [26] differ from single graphene sheet structures as they consist of multiple graphene layers arranged in an orderly or disorderly manner. CNFs do not comprise tubular structures and often have larger diameters than CNTs. The most well-known CNF structures are the platelet type, the ribbon type and the herring-bone (or fish-bone) type consisting of stacked graphene layers, as shown in Figure 1.2a-c. The tubular multi-walled and single-walled CNT structures are shown in Figure 1.2d,e, respectively, for comparison.

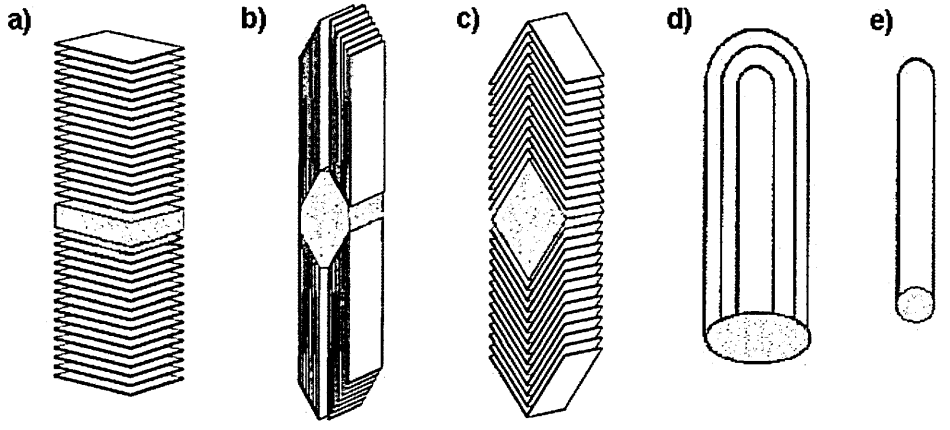

Figure 1.2 *Schematic representation of the a) platelet, b) ribbon and c) herringbone structured CNFs, as well as a d) multi-walled nanotube and a e) single walled nanotube, synthesized from metal catalyst particles [27].*

CNFs can also consist of disorderly turbostratic carbon, that is, graphite layers folded in a random manner or crumpled together [28]. The stacked graphene layers in CNFs (and pores, if available) are accessible to certain atomic and/or molecular species. As "specific surface area" is defined as the accessible surface area (active surface area) per unit mass, layered graphitic structures can enable larger specific surface areas. In the literature, CNFs have been shown to exhibit high specific surface areas of approximately $300\,m^2g^{-1}$ - $700\,m^2g^{-1}$, where the totality of the surface area is active [29,30]. However, CNFs are often described as an unwanted by-product of the catalytic reactions when manufacturing other carbon nanostructures, such as carbon nanotubes, with much effort being expended on how to prevent their formation [31].

1.3 Potential Engineering Approximations

The CNT is one of the most well-known nano-structures today and is frequently considered for applications ranging from hydrogen storage to electrodes for organic photovoltaics (OPVs). The structure of the CNT consists of a rolled-up graphene layer, capped with half a C_{60} on its tip. CNT diameters are typically between 1 nm - 50 nm and their lengths can range from a few nanometers to centimetres, leading to high aspect ratios (length to diameter ratios) and thus high specific surface areas. The measured available specific surface areas of closed MWNTs and closed SWNTs were shown to range from 110 m^2g^{-1} to 1100 m^2g^{-1} [32,33]. The maximum theoretical specific surface area for a closed SWNT is $1315\,m^2g^{-1}$ [34]. In the case of an open cap SWNT, the maximum theoretical specific surface area doubles to $2630\,m^2g^{-1}$, due to the accessible inner surface of the tube. The specific surface area of CNTs decreases rapidly with an increase in the number of walls, i.e. two walled CNTs have theoretical specific surface areas between 680 m^2g^{-1} and 850 m^2g^{-1}, whereas five walled CNTs range between 295 m^2g^{-1} and 430 m^2g^{-1} [34]. Another cause for lower

measured specific surface areas of CNTs is bundling, which theoretically decreases the available specific surface area by a factor of approximately 2, 3 and 9 for bundles of 7, 19 and 217 CNTs, respectively [34]. As bundling occurs when CNTs are sufficiently close, it is a challenge to produce densely packed, high specific surface area materials using CNT forests. The relatively high surface areas of CNTs coupled with their excellent electrical and thermal conductivities, make them ideal candidates for electrodes. Their hollow structure, low-density hexagonal lattice and high Young's modulus enables low-weight, flexible electrodes. A list of applications suggested for carbon filaments are listed in Table 1.1.

Table 1.1 *Applications of filamentous carbon nanostructures, including CNFs and CNTs.*

Electronic applications of Nanoscale carbon filaments		
Field effect transistors	Soft matter radiation detectors	Atomic force microscope tip
Conductive inks for printed circuits	Photovoltaic cells	Electrodes
Fuel cells	Gas/chemical detector	Pressure sensor [35]
Batteries	Light emitting diodes	Interconnects [36]

Multiple carbon filaments are often grown parallel and close to each other on a substrate surface, this geometry is often referred to as "forests". Strong van der Waals forces that exist at the nanoscale cause carbon filaments to attach to each other to form bundles. This decreases their effective aspect ratio, limits their useful available surface area and causes more bulk-like behaviour, which subsequently diminishes their overall efficiency as electrodes. The surface area of a CNT forest can be increased by the addition of covalently bonded molecular branches, which can approximately double the surface area to ~ 2200 m^2g^{-1} [32]. However, functionalization has detrimental effects on the electric properties of CNTs, due to the introduction of multiple heterogeneous atoms on the CNT surface, resulting in the perturbation of π electrons [37]. In addition, functionalization of CNTs using acids in high concentration can damage and fragment CNTs, decreasing their aspect ratio [37]. These problems could be solved via the use of nanostructures with different geometries that enable the separation of the nanostructures without the need for functionalization. An example geometry is that of the carbon nano-octopus (CNO), initially observed by Bernardo *et al.* in 1986 [38], which consists of multiple carbon filaments arranged radially around a single catalyst particle. The carbon filaments, or legs, are physically separated due to the geometry of the structure, inhibiting bundling. Both CNTs and CNFs have been grown this way. Each carbon structure can offer different advantages, e.g., CNTs can permit high conductivity interconnects by enabling the passage of electrons via the surface of a single rolled up graphene sheet, and carbon fibres can provide high surface areas for hydrogen storage

due to their stacked graphene sheet arrangements. However, the low CNO yields have inhibited studies on such structures for commercial applications.

1.4 Aims of Work

The National Physical Laboratory, the Advanced Technology Institute and the Medical and Aerospace Engineering department at the University Surrey have a joint interest in developing novel nanostructures for applications in electronic devices. The aims of this work are therefore to investigate the CNO geometry and its growth under multiple conditions to subsequently elucidate the growth mechanism for enabling the increase of CNO yield and the control over its physical properties. The ultimate aim is to better understand their place in industry, and more specifically, their possible role and performance as components in electrical contacts.

1.5 Structure of Thesis

Chapter 2 presents the methods of growth and describes the most plausible growth mechanism hypotheses. In Chapter 3, the sample preparation, experimental arrangements and instruments used for microscopic and spectroscopic characterisation are discussed. Surface area and electrical measurement studies are also presented, together with theoretical methods used to analyse the results. Chapters 4 and 5 present the experimental data concerning the preliminary growth of carbon nanostructures and their characterisation, including further growth experiments and more detailed characterisation. Chapter 6 is a discussion of a proposed CNO growth mechanism. Finally, in the Conclusions (Chapter 7), the work is summarised, evaluated and future work is discussed.

2 Literature Review

2.1 Introduction

The unique combination of light weight, small dimensions, excellent mechanical strength and electronic properties make carbon nano-filaments an attractive field for a wide range of applications, from reinforcing materials to molecular sensing. The physicochemical properties of carbon nano-filaments have provided a large driving force to control the growth, examine the observed properties and explore potential new applications for them. The geometry of carbon nano octopi can offer new possibilities in the fields of applied engineering and nanotechnology. The immediate problem is in reliably and reproducibly fabricating carbon nano-octopi in high yields, arising from the complex interplay between the numerous parameters integral to carbon filament growth. The growth parameters in turn affect the growth mechanism and geometry of the filaments, thus a good understanding of the filament growth will help achieving the desired yields and growth homogeneity. The growth mechanism of general carbon nano-filament structures - such as carbon nanotubes and carbon nano fibres - is discussed with no specific reference to carbon nano-octopi, owing to the lack of literature on the growth mechanism of these geometries. The literature review describes the effect of several synthesis parameters - including temperature, catalyst size and composition - on the growth of carbon filaments by a thermal chemical vapour deposition method. Subsequently, state of the art methods for achieving the growth of carbon nano-octopi are discussed.

2.2 Carbon nanostructures: synthesis techniques

2.2.1 Catalyst deposition

Catalyst deposition on substrates for CNS growth encompasses multiple methods and catalyst types. This chapter will present two main types of catalyst deposition, solution casting and physical vapour deposition. The deposition methods can be chosen on the basis that they provide different degrees of catalyst crystallinity, adhesion to substrate strength, crystal orientation, purity, thickness or particle diameter and different types of multiple metal layer configurations. These parameters in turn dictate the growth and nanostructure type that can be achieved [39].

Solution deposition methods consists of the preparation of nanocatalysts manually deposited on the surface of a sample, either via drop-casting, spin-casting or dip-casting. Drop-casting is the simplest of all methods involving a drop of the solution from a pipette onto the surface of a substrate. Spin casting makes use of a spin coater once the solution droplet has been cast on the surface of the substrate. These solution processing methods use commercial nano-catalysts and are

relatively cost effective. However, the purity of the catalysts is dependent on the manufacturing process adopted by the manufacturing company and the size, typically ≥ 50 nm, can only be partially controlled during a catalyst annealing step prior to the growth.

There exist a large number of physical vapour deposition techniques for catalyst metals, including magnetron sputtering, pulsed laser and electron beam physical vapour deposition. These allow for the deposition of thin catalyst films under vacuum conditions for applications ranging from silicon technology to metal coating for packaging in roll-to-roll manufacturing (that is the application of a coating on a roll of flexible substrate to produce a coated roll). The magnetron sputtering method is well-established and widely used in industry. Although techniques like pulsed laser deposition can achieve a better control over monolayer deposition, magnetron sputtering is often preferred owing to its wide spread use and its relatively short and inexpensive processing duration. The process of sputtering involves the insertion of a substrate to be coated in a vacuum chamber, facing a target of the material to be sputtered. The chamber is evacuated to 10^{-7} Torr and filled with argon gas, which is subsequently ionised (with a positive charge). Magnets located behind the targets trap secondary electrons from the ionisation process, which travel perpendicular to the magnetic field in a spiral-like fashion ionising further the argon atoms near the metal target. The positively charged argon plasma is strongly attracted to the negatively charged metal target (at ~ - 300 V) and impacts on the target surface, removing some atoms. The neutrally charged metal atoms originating from the target diffuse towards the substrate below to form a metal coating on the substrate surface. The increased ionisation provided by the magnets increases the concentration of the argon plasma ten-fold and therefore accelerates the rate of deposition at lower gas pressures [40]. The argon gas lightly dopes the deposited film, however, this effect is often insignificant. The deposited films produced are strongly attached to the substrate and the film thickness control is relatively accurate.

2.2.2 Chemical vapour deposition (CVD)

The most commonly used method for producing large quantities of CNTs at industrial scale and at low cost is the chemical vapour deposition (CVD) method. This method differs from the physical vapour deposition method, as the solid material deposited results from chemical reactions between a gas and a heated material [41]. A CVD system must be equipped with a supply of the reactant (gas liquid or solid), a reactor (consisting of a furnace with accurate temperature control and a substrate), and gas handling equipment, such as mass flow controllers (MFCs). A MFC is equipped with a mass flow sensor, which provides an accurate reading of the flow rate of the input gas, and adjusts the gas flow rate to that set by the operator. The main advantages of the CVD process are the high deposition rates and the variety of chemical species that can be used. The coatings tend to

be dense and homogeneous, with high adhesion to the substrate. However this procedure requires a vacuum, relatively high temperatures and often uses corrosive and explosive gases, such as acetylene.

Fibres have been formed by the catalysed decomposition of hydrocarbons for more than a century. The CVD method for the manufacture of CNTs relies on carbon atomisation via the catalytic decomposition of carbon precursors on the surface of transition metal particles, fastened on a substrate. It has been suggested that the atomized carbon diffuses through the catalyst particle. Once the solubility limit of carbon in the metal particle is reached, either by reaching a given temperature or by lowering the solubility limit by decreasing the temperature, supersaturation occurs. At this point, a solid precipitate of carbon forms, the geometry of which is dependent on the particle size and the precipitation rate [42]. Although multiple literature accounts support this growth hypothesis, this mechanism has been challenged, as it fails to explain some aspects of the growth.

Some carbon filament physical properties, such as their length and growth rate, are dependent on the experimental parameters used, such as the growth time, deposition pressure, carbon precursor concentration and temperature, see Figure 2.1. Chhowalla *et al.* [43] demonstrated that at a threshold growth duration, the carbon filaments stop lengthening due to catalyst deactivation. This occurs due to the full encapsulation of the catalyst surface by carbon deposits (discussed in later chapters). Also, the length of carbon filaments will increase with increasing deposition pressure, owing to the larger quantity of carbon available (Figure 2.1b). The length of the CNTs is not linearly dependent with precursor concentration (Figure 2.1c), as the length of the CNTs will reach a peak at 30 % acetylene concentration in the gas carrier, and will then decrease with increasing precursor concentration. This is because vertical CNT growth cannot keep up with the carbon extruded to the top so that lateral growth prevails, and short, large diameter pyramid-like carbonaceous structures form. The growth rate plotted against temperature, shown in Figure 2.1d, reaches a peak at 700 °C, but subsequently decreases with increasing temperatures. These studies also show that the CNT crystallinity increases with increasing temperature (range 500 °C - 750 °C) [44]. This is due to higher carbon mobility at higher temperatures, where carbon rearrangement enables the reconstruction of defects. Another study, by Ohashi *et al.* [45], showed that at temperatures between 900 °C and 950 °C the crystallinity of the nanotubes decreases.

The growth parameters for specific properties of CNTs (e.g. length, diameter, crystallinity) vary for different CVD systems, and need to be investigated for the particular conditions to be used. It is important to note that the growth rate can differ dramatically from experiment to experiment, some CNTs ending their growth after 3 minutes and some taking longer than 30 minutes to reach their maximum length [46]. This phenomenon is attributed to different CNT growth mechanisms that

occur as a result of the type of catalyst and the growth parameters used, as discussed in section 2.2.3.

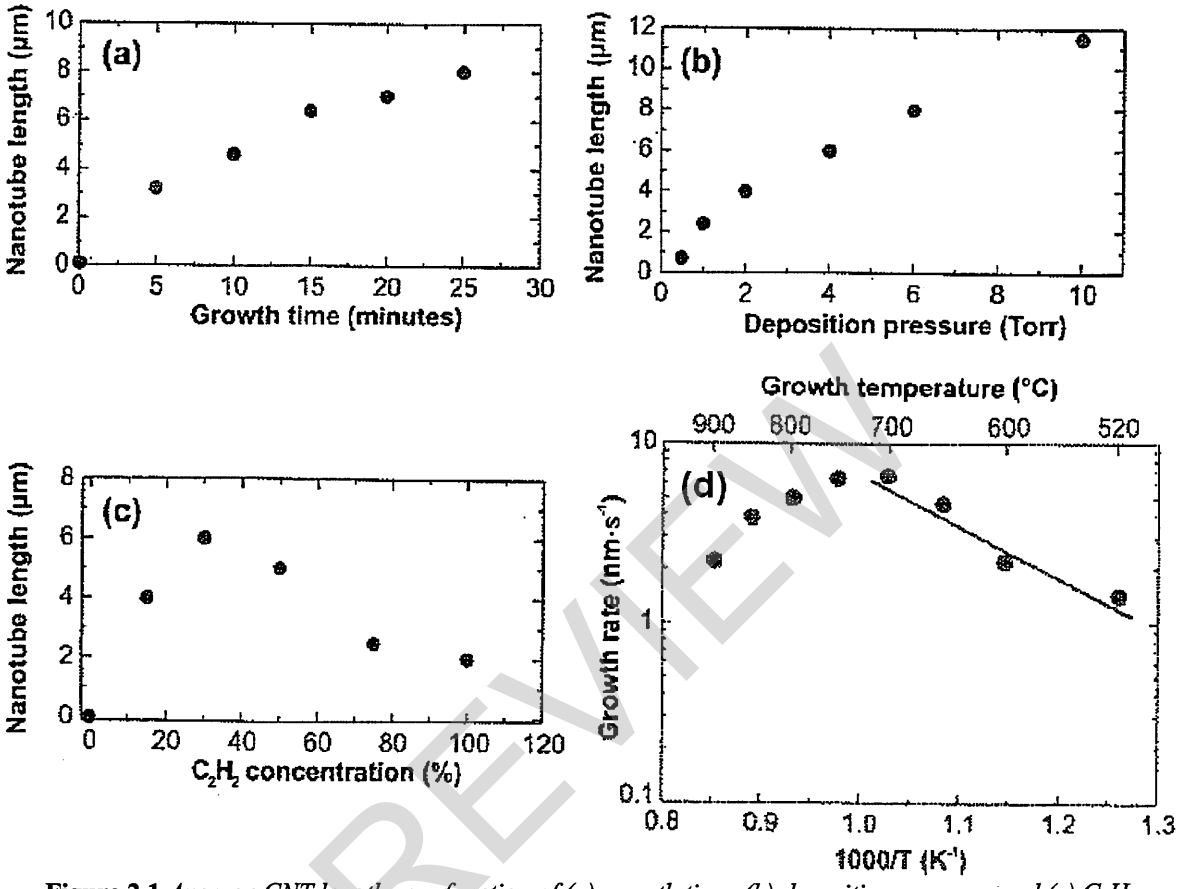

Figure 2.1 *Average CNT length as a function of (a) growth time, (b) deposition pressure and (c) C_2H_2 concentration, (d) shows the growth rate against growth temperature, after reference [43].*

The type of carbon nanostructure is also dependent on the temperatures used. For example, a temperature range of 550 °C - 750 °C is often expected to grow multi-walled carbon nanotubes, and a temperature range of 850 °C - 1000 °C tends to produce single wall nanotubes, as it is easier to achieve higher strains for small diameter tubes [47]. Gases, such as hydrogen, can be used to select the structure of a nanofilament, such as carbon nanotubes or carbon nanofibres. Low concentrations of hydrogen or none at all are more likely to produce CNTs. In contrast, higher hydrogen concentrations enable the formation of CNFs by stabilising the edges of graphene with hydrogen bonds [61].

The following sub-sections will explore some general nanostructure growth mechanisms while concentrating, wherever possible, on the specific parameters used for the CNS growth described in the experimental methods chapter (Chapter 3).

2.2.3 Growth mechanism

D'Arcy Thompson (1917) stated that the form of an object is a diagram of its growth forces [48]. In the same way, the shape of carbon nanostructures depends on the energies contributing to their growth. Often, however, this relationship between energy and form is complex and difficult to determine. Despite a large body of literature on the subject, no definitive model for the growth of carbon nanofibres has evolved, owing to a lack of consistent experimental data [49] and the large number of variables used. Considering the substantial impact that these materials are likely to have on technology, it seems imperative that their growth mechanisms be understood, so that nanofibres can be manufactured with well-defined characteristics.

In general, the most well-known CNS growth mechanisms involve the diffusion of the carbon based gas to the metal nanocatalyst surface, its subsequent adsorption, metal carbide bond formation and finally the desorption of carbon from the catalyst surface. In other words, this growth process ensures the dissociation of carbon from the gaseous compounds by the nanocatalyst to form atomic carbon, which consequently crystallises to form CNSs [50]. This process is more generally known as heterogeneous catalysis, as the phase of the catalyst (solid phase) differs from that of the reactants (gas phase). More specifically, the reaction is known as the catalytic dehydrogenation of hydrocarbons, due to the dissociation hydrogen from hydrocarbon feedstock facilitated by the activation energy (kinetic barrier) decrease by a catalyst. Transition metals like nickel, iron and cobalt are those typically used as catalysts for CNS growth. The ability of these metals to produce high throughput CNSs is attributed to the following factors: a) good catalytic activity for the decomposition of volatile carbon compounds, b) the ability of the transition catalyst to form metastable carbides (described in more detail later in this chapter), and c) the rapid carbon diffusion on their surface and through their bulk [51]. The efficacy of transition metals is attributed to their incomplete d-subshells and unpaired electrons in the ground state, which allow them to more readily bond to carbon, forming metal carbides [52]. As an example nickel has an electron configuration of [Ar] $4s^1\ 3d^9$, where the d-shell lacks a single electron [53]. Copper on the other hand, also a transition metal, has a full d-shell with an electron configuration of [Ar] $4s^1\ 3d^{10}$. However, the most common ion state of copper is Cu^{2+} with an incomplete d-shell, thus it is considered a transition metal.

For a clearer, more complete picture on CNS growth, it is possible to subdivide the mechanism into five sequential steps: a) the diffusion of precursors through a thin boundary layer to the catalyst, b) the adsorption of reactive species onto the catalyst particle's surface, c) the surface reactions leading to gaseous formation and gaseous by-products, d) the desorption of gaseous product species from the surface, e) the diffusion of outgassing species through the boundary layer

into the bulk system [47] and finally f) the deactivation of the catalyst surface via its encapsulation by a carbon layer, leading to the end of the CNT growth [26].

As can be seen from Figure 2.5 the hydrocarbons or radicals in the CVD chamber decompose into carbon and hydrogen upon contact with the catalyst surface. The carbon then dissolves and diffuses into the catalyst particle. When the carbon is supersaturated into the catalyst, it assembles to form a carbon sp^2 tubular structure that grows out of the catalyst particle.

The mechanism of growth described above refers to the vapour-liquid-solid (V-L-S) mechanism, where the vapour, liquid and solid states are those of the carbon before, during and after interacting with the nickel catalyst, respectively. The V-L-S mechanism was initially proposed by Wagner (1964) for silicon nanowire growth, and subsequently proposed by Baker (1972, [54]) in the context of carbon nanostructures. Baker described an exothermic decomposition of the hydrocarbons on an exposed facet of the metallic catalyst particle (metal/gas interface) and an endothermic carbon precipitation reaction on the opposite face of the particle (graphite/metal interface). The hypothesis states that the temperature difference between the top and the rear of the catalyst forms a temperature gradient which drives the carbon to diffuse to the cooler catalyst region, where the carbon precipitates from solution. The entirely thermodynamic approach suggested by Baker did not involve chemical bonding (between carbon and the metal catalyst) in the kinetics of the growth. Baker showed evidence that carbon diffusion through the catalyst may have been the only transport mechanism required to get the carbon from one side of the catalyst to the other. The evidence constituted the remarkable agreement between the activation energy derived from the filament growth rate, and the activation energy for the diffusion of carbon through the catalyst metal used in his experiments (1.50 eV and 1.43 eV to 1.51 eV, respectively, for an acetylene and nickel system [55]). The diffusion of carbon was, at the time, viewed as the rate determining step in the kinetics of the growth. The activation energy associated with the growth rate was found by the gradient of the natural logarithm of the growth rate plotted against the reciprocal of the growth temperatures. This followed from an Arrhenius equation relating the growth rate (increase in filament length per unit time) r, to the pre-exponential factor (or prefactor) r_0 and the activation energy E_A (Equation 2.1):

$$r = r_0 e^{-\frac{E_A}{k_B T}} \qquad \textbf{2.1}$$

taking natural algorithms on both sides gives:

$$\ln(r) = -E_A \frac{1}{k_B T} + \ln(r_0) \qquad \textbf{2.2}$$

Alstrup (1988) argued that there was indeed chemical bonding occurring in the growth process,

involving surface metal carbide formation, subsequently decomposing into filamentous carbon and metal. Both metal carbide formation and thermally activated carbon diffusion were reasonable explanations for how carbon could propagate through the catalyst. However, the physical state of the catalyst during the growth process was unclear, since some of the growths were observed to occur below the melting point of the catalyst metal. Carbon is sufficiently small so that with sufficient energy (equal or above the self-diffusion activation energy), it can diffuse interstitially through a solid metal via vacancies, grain boundaries or a melted medium. Where the catalyst is solid during the growth process, the mechanism is known as the vapour-solid-solid (V-S-S) growth. In the thermodynamic model, the fraction of the carbon deposited on the metal surface, which then enters into solution, is determined by both the solubility and the rate of diffusion of carbon in the metal. The ease of carbon diffusion through the metal is determined by the solubility of the carbon gas in the solid metal solvent. The thermodynamic solubility of carbon in the metal catalyst here is not to be confused with the growth kinetics relating to chemical reactions, such as the formation of metal carbides. Carbon solubility is dependent on carbon diffusivity, which, in turn, is temperature and metal crystal type dependent. For example, carbon diffusion in BCC Fe is 100 times greater than in FCC Fe [56], due to larger vacancies in the BCC lattice, making it easier for carbon filaments to grow on some catalyst facets than on others. The adsorption and diffusion of carbon are dependent on the crystal orientation of the catalyst facets. The (111) surface has the lowest surface energy and is therefore more likely to form on the catalyst surface. The Ni (111) surface is therefore more likely to react with the carbon feedstock owing to the higher availability of Ni(111) faces [57]. The (111) and the (110) surfaces have the lowest carbon adsorption and carbon diffusion activation energies, making them the most active sites for carbon filament growth. On the other hand, the (100) surface has a high carbon adsorption energy and a high activation energy for carbon diffusion, enabling the accumulation of carbon, which subsequently deactivates the catalyst. This computational study by Hong *et al.* [57] described how crystal domain orientation of catalyst particles plays a major role in carbon feedstock adsorption and carbon diffusion.

Hofmann *et al.* (2005, [58]) also considered a V-S-S growth mechanism and carried out a similar theoretical study to determine the location at which carbon diffusion is most likely to occur, that is, on the surface or the bulk of a solid catalyst (see Figure 2.2a,b). It was found that the adsorption energy of acetylene on a nickel (111) surface is 2.9 eV and its dissociation energy at a step edge has a magnitude of 1.3 eV as compared to a flat surface at 1.4 eV. After dissociation, the diffusion energy of atomic carbon on the nickel (111) surface was found to be 0.4 eV, and 1.6 eV in the bulk. The calculated surface diffusion activation energy on the nickel (100) surface was higher compared to all the other facets, at 1.9 eV. However, the sub-surface diffusion of carbon was predicted to be lower at 1.0 eV. It was concluded by Hoffman *et al.* that the activation energy of